APR 2 5 2005

REPORT DOCUMENTATION PAGE	Form Approved OMB No. 0704-0188

Public reporting burden for this collection of information is estimated to average 1 hour per response, including the time for reviewing instructions, searching existing data sources, gathering and maintaining the data needed, and completing and reviewing the collection of information. Send comments regarding this burden estimate or any other aspect of this collection of information, including suggestions for reducing this burden, to Washington Headquarters Services, Directorate for Information Operations and Reports, 1215 Jefferson Davis Highway, Suite 1204, Arlington, VA 22202-4302, and to the Office of Management and Budget, Paperwork Reduction Project (0704-0188), Washington, DC 20503.

1. AGENCY USE ONLY (Leave blank)	2. REPORT DATE 21.Apr.05	3. REPORT TYPE AND DATES COVERED THESIS

4. TITLE AND SUBTITLE	5. FUNDING NUMBERS
EFFECTS OF LIQUID SUPERHEAT ON DROPLET DISRUPTION AND VAPORIZATION IN SUPERSONIC CONDITIONS	

6. AUTHOR(S)
2D LT PHARISS MARK R

7. PERFORMING ORGANIZATION NAME(S) AND ADDRESS(ES) UNIVERSITY OF WASHINGTON	8. PERFORMING ORGANIZATION REPORT NUMBER CI04-1043

9. SPONSORING/MONITORING AGENCY NAME(S) AND ADDRESS(ES) THE DEPARTMENT OF THE AIR FORCE AFIT/CIA, BLDG 125 2950 P STREET WPAFB OH 45433	10. SPONSORING/MONITORING AGENCY REPORT NUMBER

11. SUPPLEMENTARY NOTES

12a. DISTRIBUTION AVAILABILITY STATEMENT Unlimited distribution In Accordance With AFI 35-205/AFIT Sup 1	12b. DISTRIBUTION CODE

13. ABSTRACT *(Maximum 200 words)*

14. SUBJECT TERMS	15. NUMBER OF PAGES 87
	16. PRICE CODE

17. SECURITY CLASSIFICATION OF REPORT	18. SECURITY CLASSIFICATION OF THIS PAGE	19. SECURITY CLASSIFICATION OF ABSTRACT	20. LIMITATION OF ABSTRACT

University of Washington

ABSTRACT

Effects of Liquid Superheat on Droplet Disruption and
Vaporization in Supersonic Conditions

Mark R. Phariss

Chair of the Supervisory Committee:
Associate Professor James C. Hermanson
Department of Aeronautics and Astronautics

Individual neat 70μm diameter droplets of 1-propanol,
ethanol, and methanol, were smoothly accelerated after
injection into a convergent-free expansion test section of
a draw-down supersonic wind tunnel to examine the effects
of liquid superheat on droplet disruption and vaporization.
Superheating of the initially unheated droplets was
accomplished upon injection into the freely expanding jet
as the static pressure dropped below the vapor pressures of
the droplet fluids. The rate and degree of superheating of
the droplets varied with test fluid vapor pressure.
Droplets were imaged by shadowgraphy over sufficiently
short intervals to capture clear images. A simple
computational model suggested that the droplets achieved
supersonic velocities relative to the air stream.
Examination of 888 droplet images indicates that

superheating results in faster and more violent disruption and vaporization than would be expected based upon correlations from previous studies, due to flash vaporization originating in the region of low pressure on the aft of the droplet. More rapid superheating seems to increase the speed and violence of droplet breakup, and result in lower degrees of superheat necessary to completely disrupt a droplet.

EFFECTS OF LIQUID SUPERHEAT ON DROPLET DISRUPTION AND VAPORIZATION IN SUPERSONIC CONDITIONS

Mark R. Phariss

A thesis
submitted in partial fulfillment of the
requirements for the degree of

Master of Science in Aeronautics and Astronautics

University of Washington

2005

Program Authorized to Offer Degree:
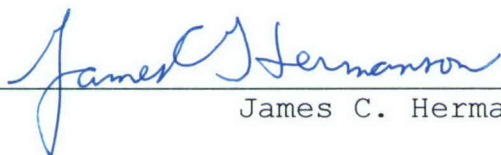Aeronautics and Astronautics

University of Washington
Graduate School

This is to certify that I have examined this copy of a
master's thesis by

Mark R. Phariss

and have found that it is complete and satisfactory in all
respects, and that any and all revisions required by the
examining committee have been made.

Committee members:

_____
James C. Hermanson

_____
Mitsuru Kurosaka

Date: 4 April 2005

TABLE OF CONTENTS

LIST OF FIGURES

LIST OF TABLES

NOMENCLATURE

English

a .... acceleration

D .... diameter

F .... force

Fo .... Fourier number

K .... coefficient

Oh .... Ohnesorge number

P .... pressure

S .... degree of superheat

t .... time

v .... velocity

We .... Weber number

x .... position downstream of throat

Greek

α .... thermal diffusivity

Δ .... change

μ .... viscosity

ρ .... density

σ .... surface tension

Subscript

c .... critical

D .... drag

d .... droplet

f .... final

i .... initial

max .... maximum observed

r .... relative

v .... vapor

0 .... initial

∞ .... freestream

PREFACE

The views expressed in this article are those of the author and do not reflect the official policy or position of the United States Air Force, Department of Defense, or the U.S. Government.

ACKNOWLEDGEMENTS

INTRODUCTION

Classic air-breathing aeropropulsion technology is approaching its theoretical flight envelope limit. Subsonic combustion ramjets, while practical, are ineffective above Mach 5;[1] rockets, while effective above Mach 5, accelerate slowly at liftoff and are not economically feasible for atmospheric flight below Mach 10.[2] The flight regime between Mach 5 and 10 would most efficiently be accessed with a supersonic combustion ramjet or scramjet.[3] This would enable hypersonic bombers or missiles for responsive airpower, as well as hybrid scramjet launch vehicles which use rockets for orbital injection to give inexpensive access to space.[2]

Current scramjet-powered research vehicles are fueled by either liquid hydrogen or preheated hydrocarbons.[4] The short autoignition delay and high reaction rate of hydrogen is desirable, since the residence time of the fuel-air mixture in the combustion section can be less than the autoignition delay of hydrocarbons.[5-6] Liquid hydrogen is cryogenic and therefore readily vaporized, avoiding the need to vaporize in the combustion chamber.[2] Additionally, since hydrogen molecules are less massive than hydrocarbon molecules, exhaust velocity at a given combustion

temperature is higher when hydrogen fuel is used. One major drawback of liquid hydrogen is that the fuel is not storable,[2] which prevents economical ground operations, sacrificing a major advantage of using scramjet-powered vehicles in place of rockets for high speed atmospheric flight.

An alternative to hydrogen is provided in hydrocarbon fuels. Hydrocarbons can be used as coolant for the engine, especially when catalytically cracked,[7] which also lowers the autoignition delay time.[6,8] In addition, the higher volumetric energy density of hydrocarbons reduces structural mass necessary for fuel storage and radar cross section of the vehicle.[2,9] The hurdles for fueling a scramjet with hydrocarbons are only of implementation. Preheating of hydrocarbons to inject vapor instead of liquid involves either bulky heat exchangers[4] or dangerously volatile starter fuels.[1]

Without specialized equipment or chemicals to preheat hydrocarbon fuel at engine start, hydrocarbon fuel may injected as a liquid in a "cold start" situation,[10] in which the fuel is unheated upon injection into the combustion chamber. Indeed, for an operational scramjet, hydrocarbons injected as liquid may in fact be more efficient for fuel-

air mixing than vapor injection. Since liquid, due to its higher momentum, can penetrate into a cross flow better than vapor,[11] the optimal design may involve injecting liquid hydrocarbon fuel into the combustion chamber and rapidly vaporizing the fuel after its injection. Once vaporization of liquid fuel is sufficiently fast, the mixing of the fuel vapor and air becomes the limiting factor in combustion rate.

Superheating hydrocarbon fuels has the potential to achieve this rapid vaporization, as superheated liquids rapidly evaporate throughout the bulk of the liquid.[12-13] Due to the inevitable presence of boiling nucleation sites on the surface of fuel tanks,[13-15] superheating would necessarily be best accomplished upon injection, where the microscopically smooth fluid-fluid boundary between the airflow and fuel would deny nucleation sites that could lead to slow, cold heterogeneous boiling,[13-14] while allowing for rapid evaporation of the bulk liquid. In addition, the amount of superheat could be increased by exposing the fuel, during injection, to a rapid drop in pressure below the vapor pressure of the fuel.[14]

Whether the liquid is injected as a jet or a spray,[16] a critical stage of fuel vaporization is breakdown and

vaporization of individual droplets.[10] Numerous studies have examined aerodynamic shattering of droplets and correlated the mode of and time to disruption with various non-dimensional parameters.[17-35] The most common of these parameters are the Weber number:

$$We = \frac{\rho_\infty \cdot v_r^2 \cdot D_0}{\sigma},$$

which relates inertial forces to surface tension; the Ohnesorge number:

$$Oh = \frac{\mu_d}{\sqrt{\rho_d \cdot \sigma \cdot D_0}},$$

which relates viscous forces to surface tension; and the Reynolds number:

$$Re = \frac{\rho_\infty \cdot v_r \cdot D_0}{\mu_\infty},$$

which relates inertial forces to viscous forces.

Various modes of droplet breakup under non-superheated conditions have been identified differently by various studies.[17-20,35-36] The most common major modes, in order of increasing violence, are vibrational, bag, stripping, and catastrophic. Fig. 1.1 depicts the typical evolution of each of these modes. Additionally, Weber number ranges correlated to these modes, and other modes that have sometimes been reported[21] are depicted. A droplet

undergoing vibrational breakup oscillates and, if there is sufficient energy transfer from the flow, the amplitude of the oscillations increases until it exceeds the size of the droplet, at which point the droplet separates into two or more smaller droplets. At higher rates of energy transfer from the flow to the droplet than in the vibrational mode, the airflow non-oscillatorily pierces the windward side of the droplet, deforming it into a bag shape, which thins until the airflow pierces completely through the droplet, at which point the droplet fragments progressively from the point of piercing until the leading ring is broken into several droplets. At even higher flow to droplet energy transfer, the shear on the surface of the droplet strips away some of the liquid as a vapor; as the energy increases, this shear can also create waves on the surface of the droplet, accelerating the stripping of liquid. The final commonly defined mode, catastrophic breakup, occurs when the energy transfer from the flow to the droplet is sufficient to create waves on the surface of the droplet with amplitudes greater than the size of the droplet, rapidly disintegrating the droplet into several small fragments which subsequently also undergo catastrophic breakup.[20]

Most previous studies of droplet breakup have focused on either low-speed flow with smooth application of aerodynamic loads to droplets,[20-24] or high-speed flow with sudden application of aerodynamic loads to stationary droplets in a shock tube.[17-18,25-31,34] The smooth application of aerodynamic loads to droplets in high-speed flow is insufficiently characterized by the results of previous studies, as the rate of aerodynamic loading and speed of flow affect droplet breakdown considerably.[16-17,32-33] In addition, these studies have largely ignored thermodynamic factors of breakup, such as superheating of droplets. One recent study, which explored the effects of superheat on droplets accelerated to high subsonic relative velocities, suggested that increasing superheat decreases time to disruption of droplets and increases the violence of breakup for a given value of Weber number.[10]

The current research investigates the effect of superheat on the nature of and time to breakup of liquid droplets smoothly accelerated to supersonic relative velocities, through visual shadowgraphy of droplets of various test fluids with a range of vapor pressures in a freely expanding jet test section of a draw-down supersonic wind tunnel.

a) VIBRATIONAL BREAKUP
We ≤ 12

FLOW

b) BAG BREAKUP
12 ≤ We ≤ 50

FLOW

DEFORMATION   BAG GROWTH   BAG BURST   RIM BREAKUP

c) BAG-AND-STAMEN BREAKUP
50 ≤ We ≤ 100

FLOW

a) SHEET STRIPPING
100 ≤ We ≤ 350

FLOW

b) WAVE CREST STRIPPING
350 ≤ We

FLOW

c) CASTASTROPHIC BREAKUP
350 ≤ We

FLOW
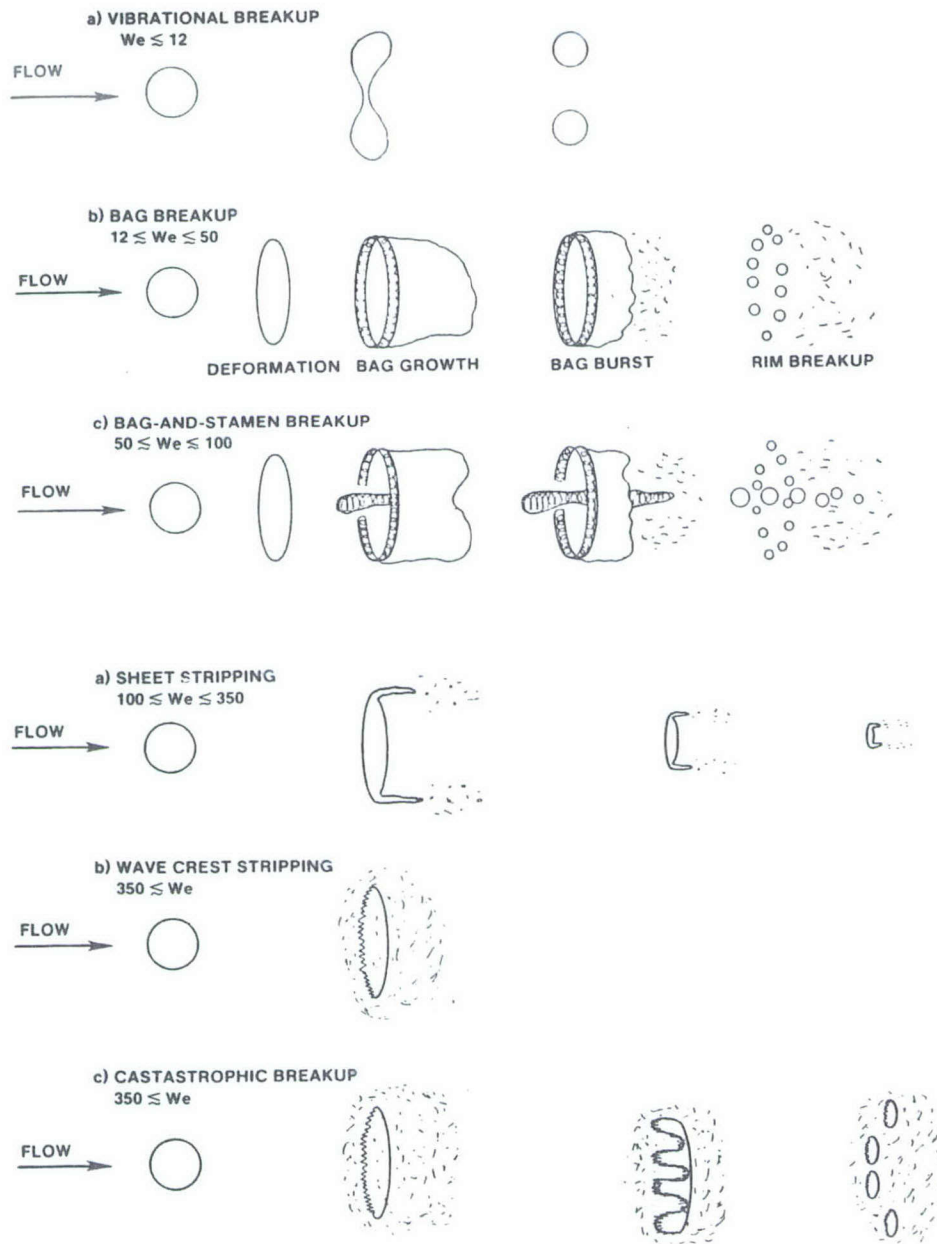
Figure 1.1 Droplet Breakup Modes[21]

EXPERIMENTAL

Wind Tunnel

The experiments were conducted in the draw-down
Supersonic Wind Tunnel at the University of Washington. At
operating condition with atmospheric pressure of 14.7 psia
(101.35 kPa), the vacuum pump maintained a tank pressure of
1.2 psia (8.27 kPa). A photograph of the test section
exterior is shown in Fig. 2.1; a diagram of the test
section interior and nozzle contour is shown in Fig. 2.2.
In order to achieve the most rapid droplet acceleration, a
freely expanding jet was employed. The convergent section
is 0.625 in (15.875 mm) long with a 1 in (25.4 mm) diameter
entrance, and a 0.125 in (3.175 mm) diameter throat. The
interior shape is a right conic frustum. The interior of
the test section is a cube with a side of 3 in (76.2 mm)
with the convergent section protruding 0.25 in (6.35 mm)
down from the center of the top. Circular quartz windows
with diameters of 1.57 in (40 mm) are mounted on opposite
sides of the test section to allow for shadowgraph
illumination and imaging of the entire expansion cell from
throat to Mach disc. The airflow freely expanded from Mach
1 at the throat to Mach 4.87 at the end of the expansion

cell. The Pitot pressure along the centerline of the test section was measured with a Pitot probe inserted from the bottom of the tunnel; from this, the Mach number, velocity, static temperature, and static pressure were calculated as a function of position downstream of the throat, as shown in Figs. 1.3, 1.4, 1.5, and 1.6, respectively.

Droplet Generation Apparatus

A *MicroFab* Droplet-on-Demand device, pictured in Fig. 2.7, was used to generate monodisperse 70 μm (0.0028 in) diameter droplets of each test fluid. When triggered by a voltage pulse from a *MicroJet III* controller, a piezoelectric transducer in the device creates an acoustic wave in a fluid filled chamber which interacts with the free surface at the tip to create a single drop per pulse.[10,37] Supplied by a syringe pump with a constant flow of test fluid equal to that expelled as droplets, the device generated a steady stream of droplets at 3000 Hz. The droplet generator was positioned 2 in (50.8 mm) above the entrance of the convergent section of the test section, and was aligned with 3-axis microstagers to ensure the droplets were injected on centerline.

Imaging System

Droplets were imaged in the test section using shadowgraphy. Illumination was accomplished with a Xenon Corp. N-787B Nanopulse system generating 500 mJ (0.12 cal) pulses 10 ns in duration at a repetition rate of 60 Hz. In a 10 ns interval, a 70 μm (0.0028 in) diameter droplet moving at 2,300 ft/s (700 m/s) — the maximum airflow velocity in the test section — moves only 10% of its diameter; therefore, the images were of droplets effectively "frozen" at a given position and state of deformation and fragmentation.

The images were captured with a Panasonic WV-CP474 CCD camera with a VZM 300 video microscope lens attached. The camera output the 480 x 640 pixel images to a *Mu-Tech* MV1000 PCI frame grabber card in a controlling PC, which recorded the images as 8-bit grayscale TIFF image files and stored them on the PC hard drive for later post-processing. Since the field of view of the camera with the microscope lens was much smaller than the length of the test section, it was necessary to step the camera down the length of the test section in order to capture images of droplets throughout their lifetime. In order to identify the location of camera fields of view below the throat, 0-80

screws of known length were rigidly held at throat and an image recorded at the field of view.

The position of the image varied by ± 31 μm (0.0012 in) due to the random nature of the path of current through the air gap at breakdown voltage. The combination of lens and CCD resulted in each pixel of the images displaying a 3.6 μm (0.00014 in) square area of the test section. Due to the error of the arc position, in both the droplet image and the image of the screw of known length, and the finite pixel size, the position of any droplet in an image is known within a range of ±69.2 μm (0.0027 in), less than its nominal injection diameter and only 0.36% of the total length of the test section.

Image Processing

Due to the combined characteristics of the CCD camera, the test section, and the light source, the unprocessed images of droplets did not normally clearly reveal features of the droplet breakup. An unprocessed image can be seen in Fig. 2.8. In order to remove these visual artifacts, a MATLAB program utilizing seven custom MATLAB functions (see Appendix) was written.

Deinterlacing

The first and simplest problem with the images was that they were interlaced, meaning the camera only used every other row to record the a given image. The image was deinterlaced by setting the value of each pixel in the dark rows equal to the average of the values of the pixels immediately adjacent in two bright rows. A deinterlaced image can be seen in Fig. 2.9.

CCD Blemish Removal

Small areas of the CCD had been damaged by dust and could not be cleaned. This left spots in the image. In order to eliminate these spots, several random images were compared. Those pixels which had a value above a critical value in all images compared were identified as damaged CCD points. The values of these pixels in processed images were set to the mean value of all the pixels in the image, effectively "graying-out" the spots, as can be seen in Fig. 2.10.

Window Blemish and Light Source Corrections

Despite careful cleaning with solvents and lint-free cloths, microscopic residue remained on the windows of the tunnel. However, due to the variation of the position of light source arc, this residue appeared at different pixels

of each image. In order to remove it, images of the test
section with no droplets were recorded at each position.
These residue-only images were compared with several copies
of each processed image with varying offsets in both axes
to compensate for the light source movement. The copy
which varied the least from the residue-only image over the
entire image had the residue-only image subtracted from it,
removing the window blemishes while also inverting the
grayscale. An example can be seen in Fig. 2.11.

Noise Reduction

The scaling of the subtracted imaged increased the
strength of the noise along with the signal of the droplet
in the image. To reduce the noise, each pixel value was
set to the arithmetic mean of its value and the values of
the twelve pixels nearest it; small exceptions were made
for the pixels near the edge of the image, whose values
were averaged with fewer neighboring pixels as there were
fewer pixels nearby. A noise reduced image can be seen in
Fig. 2.12.

Edge Sharpening

In averaging the noise out of the image, the signal of
the droplet in the image was blurred. To sharpen the edges
of the droplet image, the image was convolved with an

evenly weighted eight neighbor Laplacian kernel[38], and added with itself. A final scaling to use the entire grayscale resulted in images such as shown in Fig. 2.13.

Test Fluids

Droplets of 1-propanol, ethanol, and methanol were injected into the test section. Table 2.1 shows some fluid properties of these fluids,[39] and the Ohnesorge number for a 70 μm (0.0028 in) diameter droplet of each fluid. As can be seen, the vapor pressure values for the fluids progress in an approximate sequence of halves, leading to different degrees of superheating, defined as

$$S = \frac{P_v}{P_\infty},$$

of droplets of each fluid at a given location downstream of the throat in the test section, as shown in Fig. 2.14. This approach allows examination of the effects of superheating on disruption of droplets at comparable Weber numbers. It should be noted that for any given liquid a limiting degree of superheating exists, beyond which the liquid is absolutely thermodynamically unstable. For a given fluid, the fraction of its critical temperature at which the fluid reaches the superheat limit for a given fraction of its critical pressure can be approximated using

the Redlich-Kwong equation, as shown in Fig. 2-15.[40] Based

on the temperature of the droplets in the test section and

the static pressure, the droplets in the current study,

though superheated, do not actually reach the superheat

limit.

The calculated total residence time, based on the

model described in the next chapter, of a droplet between

the throat and Mach disc is 32.4 μs. This yields a maximum

Fourier number:

$$Fo = \frac{4 \cdot \alpha \cdot t}{D^2},$$

of approximately 0.01. This suggests cooling of the bulk

droplet fluid other than by fragmentation and vaporization

can be neglected. The Ohnesorge number progresses roughly

in an integral sequence, suggesting that a decrease in

viscosity will accompany an increase in superheat level due

to the use of a different fluid. The values of surface

tension for the three fluids vary only slightly from each

other, so the Weber number for a droplet of the same size

and velocity for each fluid will be similar. This

minimizes variation in the aerodynamic breakup forces most

often studied, allowing the focus to remain on the effects

of the liquid superheating.

Figure 2.1 Test Section Exterior
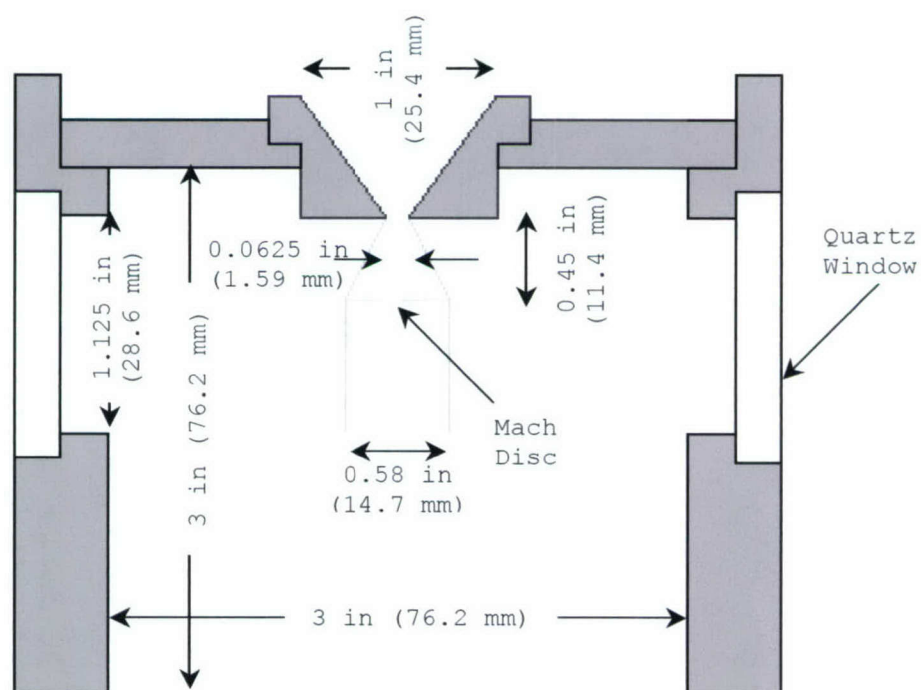
Figure 2.2 Test Section Interior
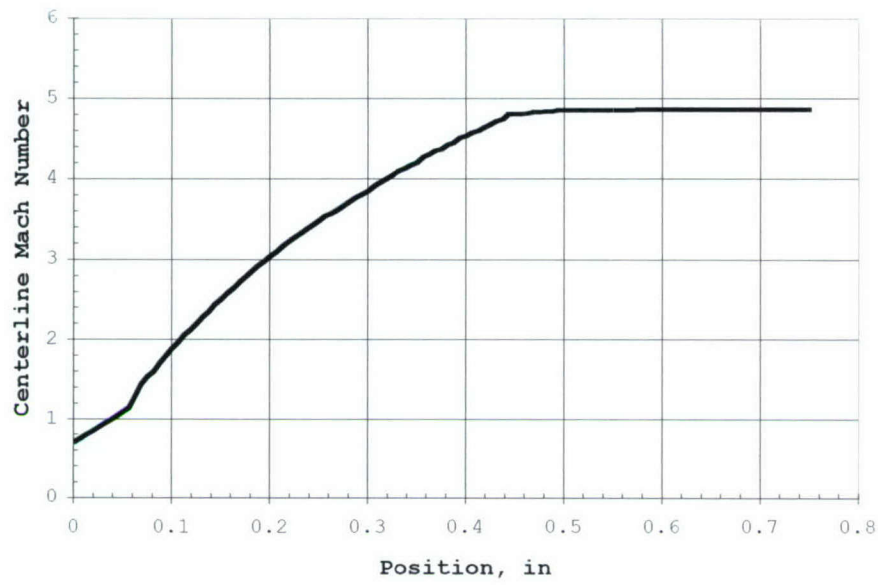
Figure 2.3 Centerline Mach Number
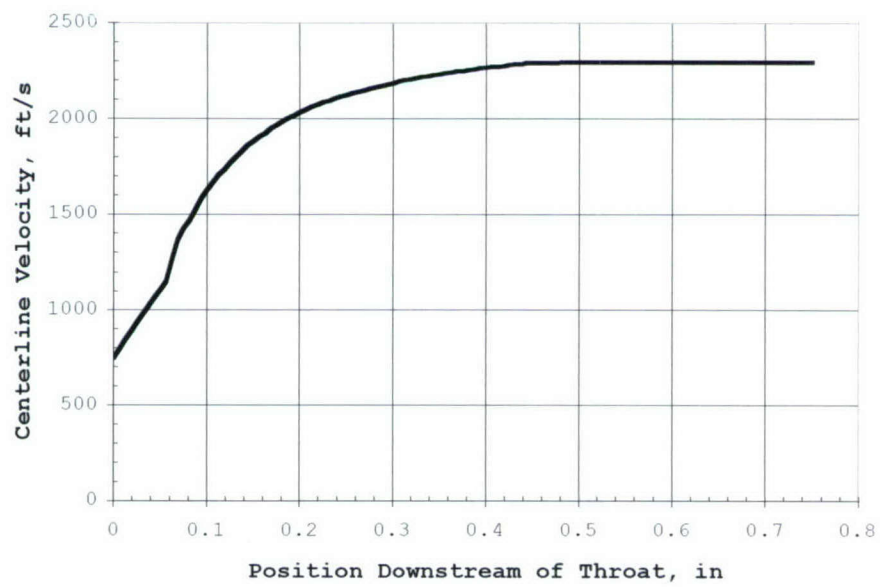
Figure 2.4 Centerline Velocity
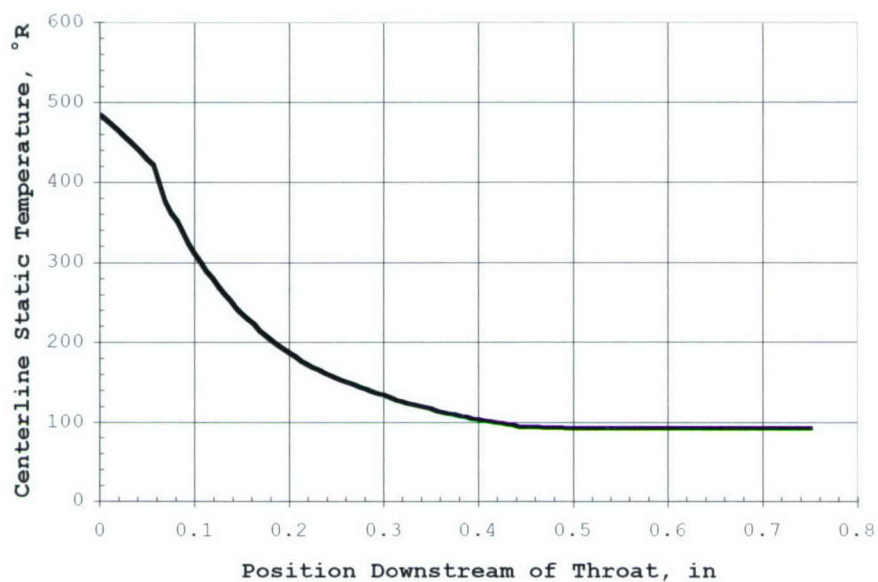
Figure 2.5 Centerline Static Temperature
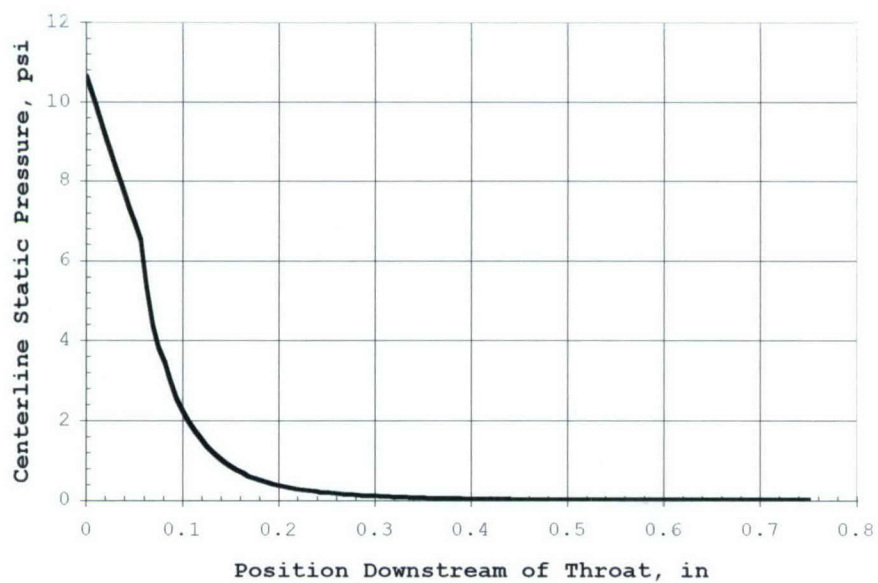
Figure 2.6 Centerline Static Pressure

Figure 2.7 Droplet Generator

5:1 Scale
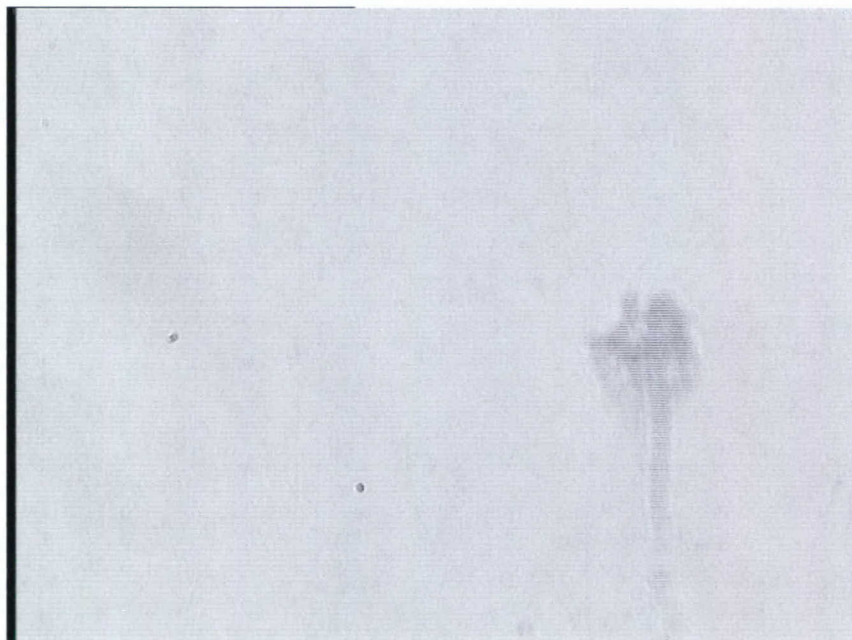
Figure 2.8 Unprocessed Droplet Image

Figure 2.9 Deinterlaced Droplet Image

Figure 2.10 CCD Blemish Removed Droplet Image
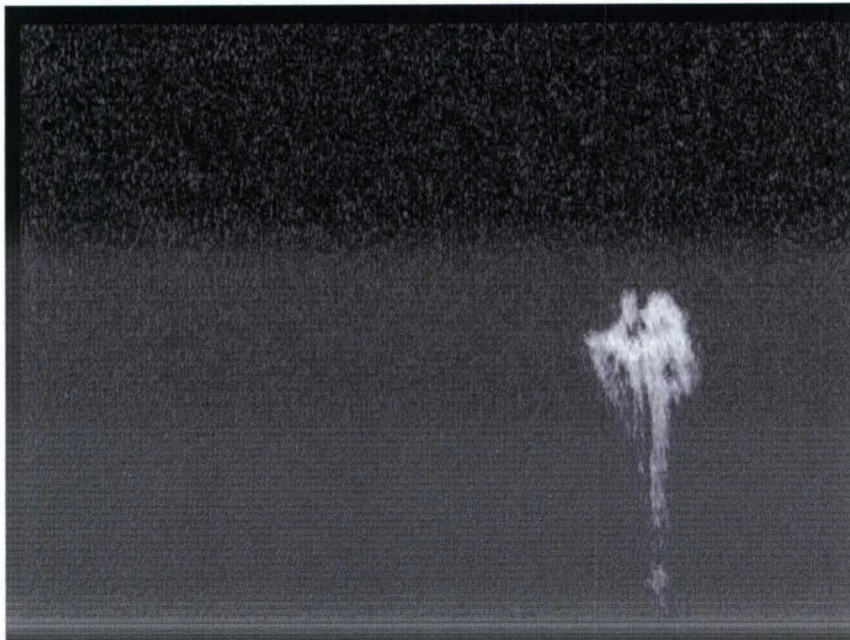
Figure 2.11 Window Blemish Removed Droplet Image
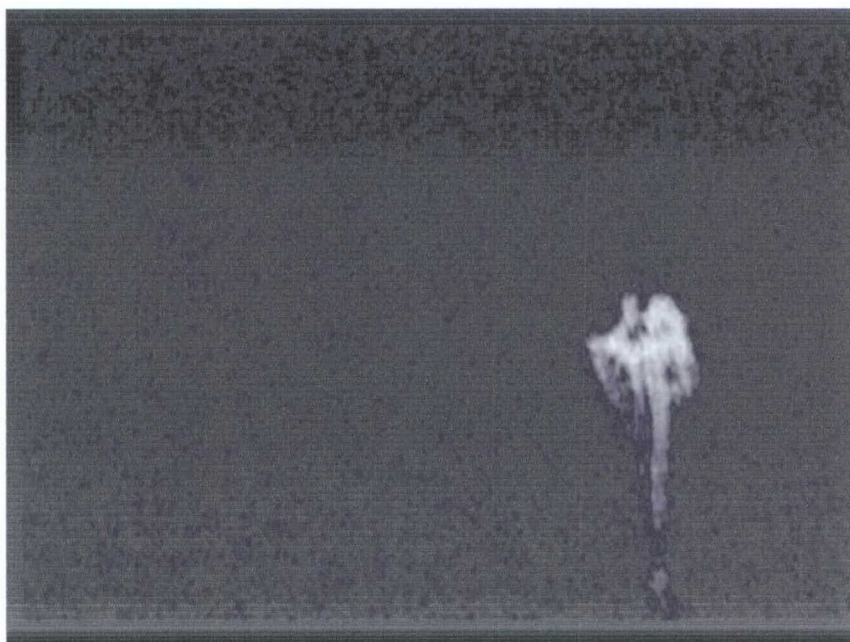
Figure 2.12 Noise Reduced Droplet Image

Figure 2.13 Fully Processed Droplet Image

Table 2.1 Test Fluid Properties

Test Fluid	P_v psi	ρ g/mL	σ dyn/cm	μ cP	Oh	T_c K
1-Propanol	0.385	0.8035	23.7	1.722	0.047165	536.8
Ethanol	0.851	0.7893	22.3	1.080	0.030768	489.2
Methanol	1.911	0.7914	22.6	0.600	0.016957	512.6
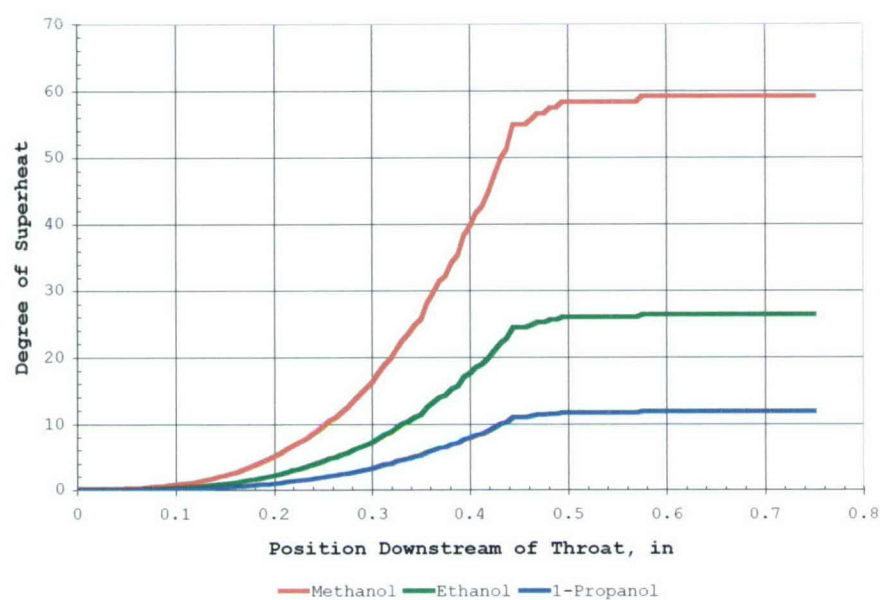
Figure 2.14 Degrees of Superheat
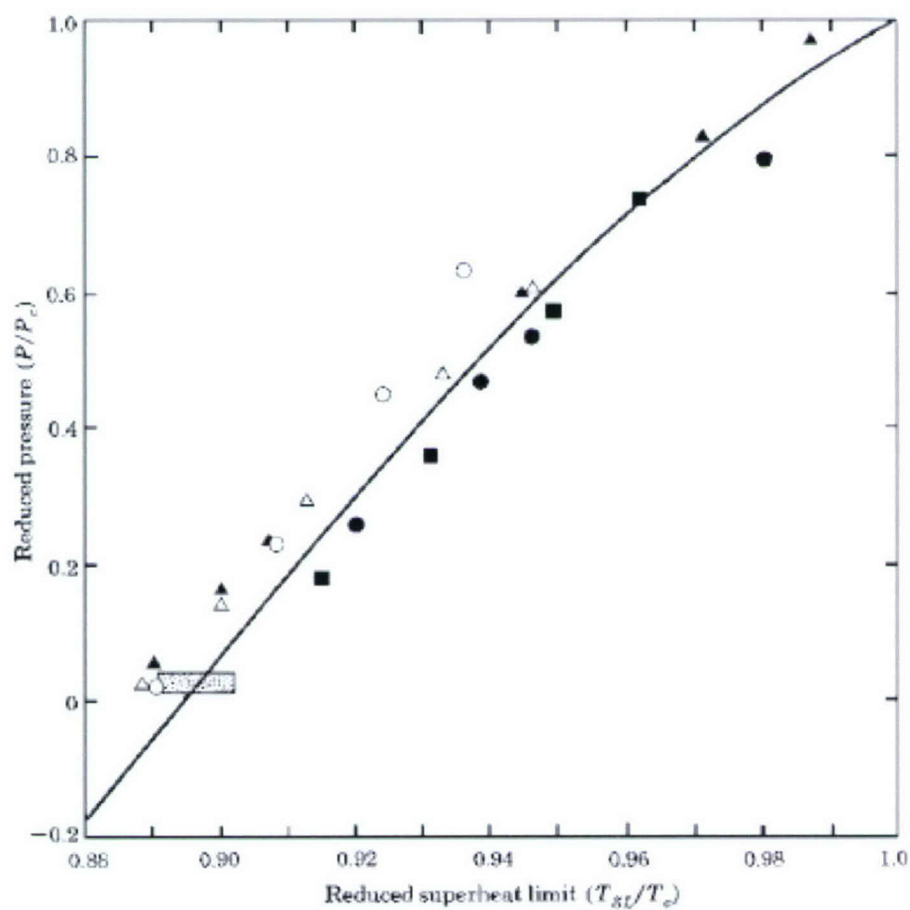
Figure 2.15 Superheat Limit Correlated to Redlich-Kwong Equation[40]

COMPUTATIONAL MODEL

A one-dimensional model of the expected acceleration of droplets injected into the test section was developed, yielding an estimate of droplet velocity. From the model velocity profile, estimates of droplet velocity and Mach number relative to the airflow were calculated. From the calculated droplet relative velocity profile, estimates of droplet Weber and Reynolds number were calculated to predict which droplet breakup regimes should be observed, based on correlations from previous studies.[17-19,21,25-27,34-36]

Model Structure

The limiting approximation of model is that the droplets are modeled as non-evaporating, rigid spheres. The reason for this assumption is to allow the use of existing drag coefficient data for small-diameter metal spheres at Mach numbers between 0.29 and 3.96. One limitation to the accuracy of the model is that the metal spheres for which the drag was correlated were smaller than the droplets considered here. The effects of compressibility on spheres on the scale of the droplets are not well established. The existing drag coefficient data are related to the drag force as follows:

$$F_D = K_D \cdot \rho_\infty \cdot D^2 \cdot v_r^2$$

The determined value of drag coefficient, as a function of Mach number, is as follows:[41]

$$K_D = \begin{cases} 0.192 & , 0 < M < 0.5 \\ 0.3173 + 0.2711 \cdot (M-1) & , 0.5 < M < 1.4 \\ 0.3812 - 0.0140 \cdot (M - 2.75), & 1.4 < M < 4.0 \end{cases}$$

The model was used to calculate droplet kinematical behavior from the tip of the droplet generator to the Mach disc at the end of the free expansion cell, for position increments of 1/160 in (0.159 mm). For the initial condition, at the first position step, the droplet velocity was taken to be half the velocity of the local airflow. The Mach number of the droplet relative to the air stream at each position step was calculated by dividing the droplet relative velocity by the sound speed for the static temperature at that position, as determined experimentally.

The relative droplet Mach number was then used with the above correlation to determine the drag coefficient, which, with the droplet relative velocity, an assumed nominal diameter of 70 μm, and the experimentally determined freestream density, was used to calculate the drag force. The drag force was divided by the product of the nominal assumed volume of the droplet and the density of ethanol to

find the acceleration, which was assumed to remain constant

across the length of each position increment; the density

of ethanol was used since the densities of the test fluids

vary only slightly, and ethanol has the median density of

the three fluids. The Newtonian equation for change in

velocity due to constant acceleration over a distance:

$$v_f^2 = v_i^2 + 2 \cdot a \cdot \Delta x$$

was used to determine the velocity at the next position

step. The process was repeated for each position step

within the length of interest.

Computational Results

The modeled indicated that the droplets accelerate

from 711 ft/s (216 m/s) at the throat to a maximum of 1465

ft/s (447 m/s) before slowly decelerating relative to the

airflow again, as profiled in Fig. 3.1. The relative Mach

number is computed to increase from 0.66 at the throat to a

maximum of 2.89, as shown in Fig. 3.2; the predicted

relative Mach number continues to increase after the

relative velocity is predicted to reach a maximum due to

the decrease in sound speed associated with the drop in

static temperature along the length of the test section.

The Weber number is predicted to be between 149 and 632, as

shown in Fig. 3.3. The Reynolds number is predicted to be between 890 and 1835, as shown in Fig. 3.4. Studies of drag on smooth spheres in incompressible flow indicate comparable drag coefficients over the range of Reynolds numbers between those predicted by the model for the droplets and those for the rigid spheres from which the drag coefficient correlation was derived,[42] suggesting that the drag coefficient correlation is sufficiently applicable to the scale of the droplets considered here. These results, based upon a rigid sphere model, provides a reference to which the experimental results, expected to differ from those of the model due to droplet deformation, disruption, and vaporization, can be compared.

Breakup Mode Predictions

Upon comparison with established correlations, the model results were used to predict the mode of droplet breakup expected. Three types of correlations were found: Weber number only, Weber and Ohnesorge numbers, and Weber and Reynolds numbers. There is some variation in the various correlations, but one dominant breakup mode was predicted by the vast majority of the correlations for the Weber, Ohnesorge, and Reynolds numbers predicted by the model for the conditions of the current study.

The Weber number only correlations[18-19,21,25-27,34] predict that the droplets will fragment, but will enter neither the bag (since We > 100)[18] nor catastrophic (since We < 20,000)[26] disruption modes. Due to the focus of these correlations on individual boundaries between breakup modes and not on the entire range of breakup modes, no more specific predictions can be confidently made from those results. The Weber and Ohnesorge numbers correlation,[17] predicts a pure shear breakup (since Oh < 0.1 and We > 78),[17] based upon the model results. The Weber and Reynolds numbers correlations predict that the droplets should initially deform, flattening the leeward surface and making the windward surface convex,[17] which when coupled with qualitative observations from other studies[22,28-29] can be used to again eliminate the bag breakup mode as a possible breakup mode expected. Other Weber and Reynolds numbers correlations[35-36] further predict that the droplets will begin fragmentation in the shear mode and transition to a final explosive disruption (since 40 < We < 1,000 and 1 < $WeRe^{-0.5}$ < 20).[36] Based upon the preponderance of the correlation predictions, coupled with the expectation that droplet acceleration will exceed that approximated in the model due to deformation and vaporization of liquid, a

shear stripping mode breakup with possible transition to

explosive but not catastrophic final disruption is expected

for the conditions of this work. Since the correlations

referenced here relate droplet breakup modes to given

values of non-dimensional parameters, regardless of

possible variation of droplet diameter, the correlations

should remain valid for fixed flow conditions since the

ranges of non-dimensional parameters calculated with this

model also assume constant droplet diameter. The validity

of using these correlations is diminished, however, due to

the continually varying velocity of the droplets relative

to the air flow in this study.
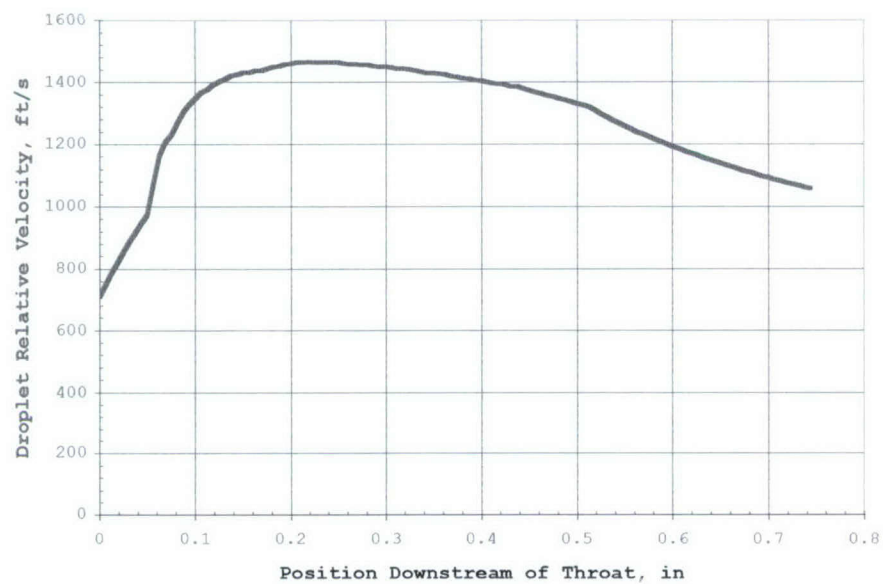
Figure 3.1 Modeled Droplet Relative Velocity
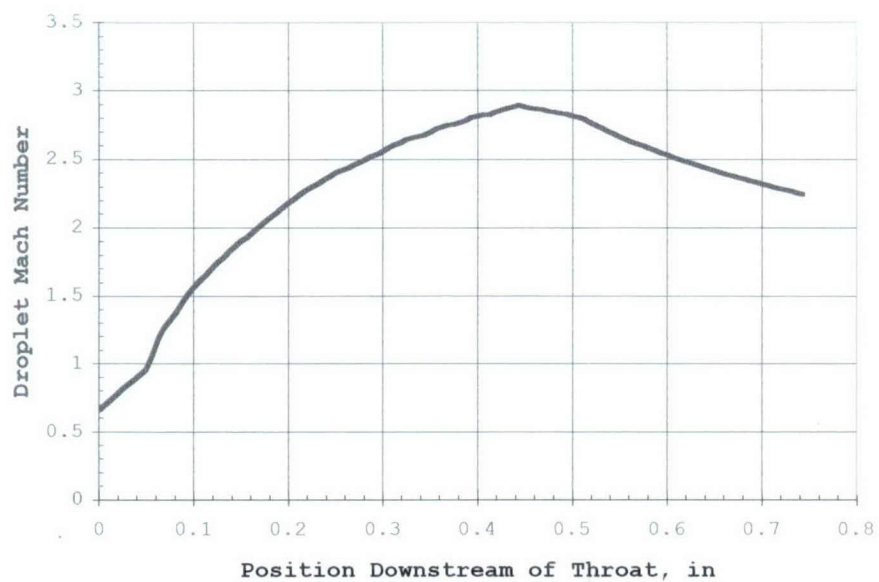
Figure 3.2 Modeled Droplet Relative Mach Number
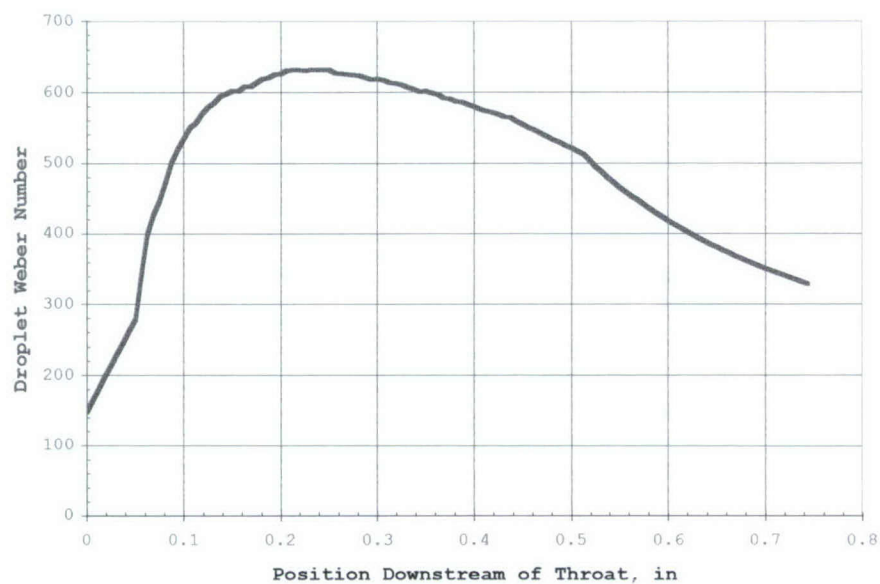
Figure 3.3 Modeled Droplet Weber Number
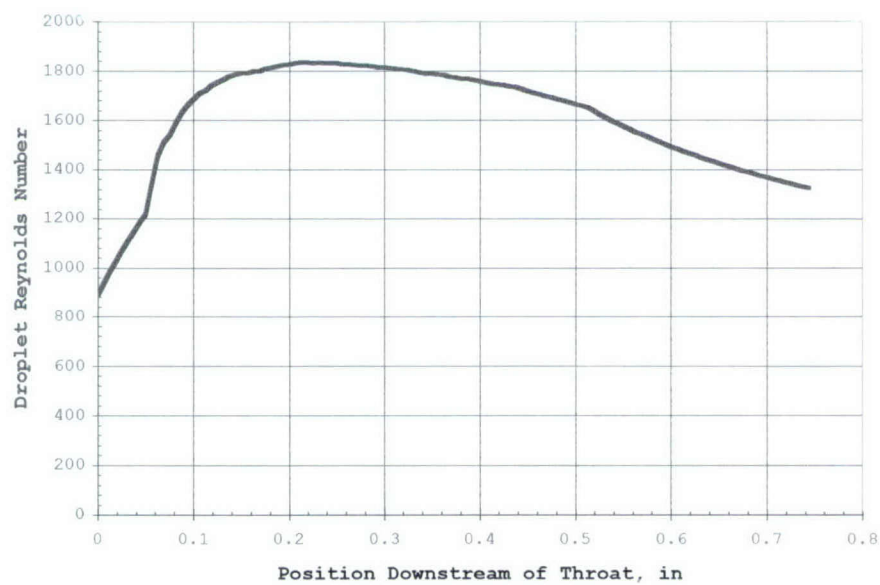
Figure 3.4 Modeled Droplet Reynolds Number

EXPERIMENTAL RESULTS

1-Propanol

Images of nine 1-propanol droplet exemplars — out of
514 1-propanol droplet images captured — for various
positions in the test section are shown in Figs. 4.1-4.9;
Table 4.1 summarizes specific information about these
droplets. The droplets seem to have initially deformed as
predicted, convex on the windward surface. The 1-propanol
droplets remained unsuperheated through Fig. 4.4, with the
deformation continuing and forming a tail at the aft of the
droplets. The onset of superheating in Fig. 4.5 appears to
have resulted in rapid disruption and vaporization, with
the initiation apparently occurring within the bulk of the
fluid. Coherent droplet fragments were observed much
farther downstream in the test section and at a much higher
degree of superheat for 1-propanol droplets than for
droplets of the other two fluids.

Ethanol

Images of six ethanol droplet exemplars — out of 241
ethanol droplet images captured — for various positions in
the test section are shown in Figs. 4.10-4.15; Table 4.2
summarizes specific information about these droplets. The

droplets in Figs. 4.10-4.12 are not superheated, and seem

to deform predominately at the aft of the droplet, in much

the same manner as the 1-propanol droplets. The droplets in

Figs. 4.13-4.15 are superheated to a quickly increasing

degree, due both to the steadily decreasing static pressure

in the test section and acceleration of the droplet

downstream by the air flow. The droplet liquid appears to

have undergone flash vaporization, possibly initiating at

or behind the separation point. Disruption occurred at a

similar degree of superheat to that at which disruption

occurred in 1-propanol droplets. Fig. 4.15 represents the

maximum downstream position of observable droplet

fragments.

Methanol

Images of three methanol droplet exemplars — out of

133 methanol droplet images captured — for various

positions in the test section are shown in Figs. 4.16-4.18;

Table 4.3 summarizes specific information about these

droplets based both on experimentally determined airflow

characteristics and computationally modeled non-dimensional

parameters. Very little structure is observable in these

droplets. Only Fig. 4.18 shows a superheated drop, but the

rate of increase of degree of superheating of the droplets

was much more rapid than for droplets of 1-propanol and ethanol. This is due both to the higher vapor pressure of methanol, and higher acceleration downstream as the droplets of methanol lost mass to vaporization more quickly than did droplets of the other fluids. No methanol droplets were observable farther downstream than Fig. 4.18.

Figure 4.1 1-Propanol Droplet at x = 0.0109 in (0.28 mm)

S = 0.0392, Model v_r = 775.7 ft/s (236 m/s), Model M_r = 0.727, Model We = 177, Model Re = 971

Figure 4.2 1-Propanol Droplet at x = 0.1109 in (2.82 mm)

S = 0.2151, Model v_r = 1373 ft/s (418 m/s), Model M_r = 1.641, Model We = 555, Model Re = 1719
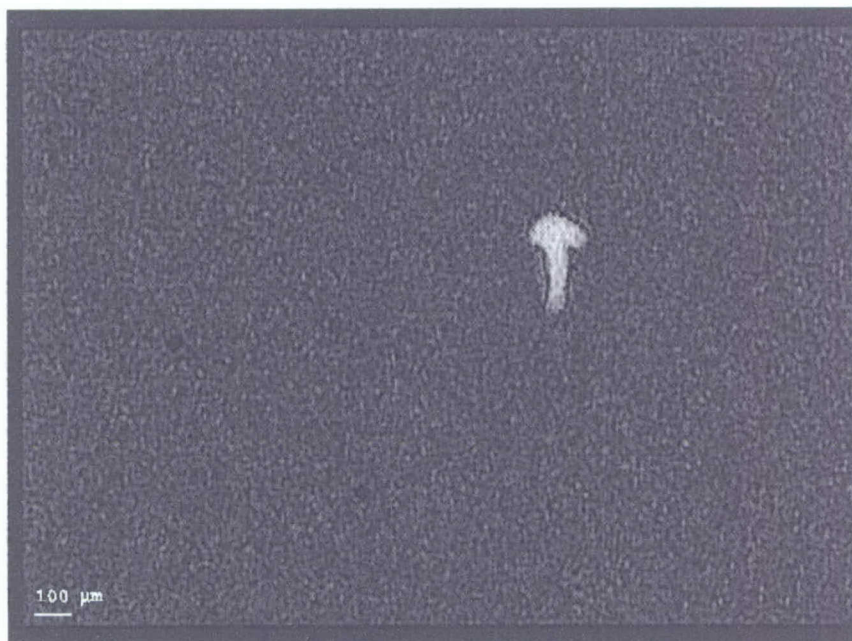
Figure 4.3 1-Propanol Droplet at x = 0.1430 in (3.63 mm)

S = 0.3989, Model v_r = 1425 ft/s (434 m/s), Model M_r = 1.861, Model We = 598, Model Re = 1785

Figure 4.4 1-Propanol Droplet at x = 0.1818 in (4.62 mm)

S = 0.7772, Model v_r = 1450 ft/s (442 m/s), Model M_r = 2.082, Model We = 619, Model Re = 1816

Figure 4.5 1-Propanol Droplet at x = 0.2622 in (6.66 mm)

S = 2.2172, Model v_r = 1459 ft/s (445 m/s), Model M_r = 2.434, Model We = 626, Model Re = 1827

Figure 4.6 1-Propanol Droplet at x = 0.3089 in (7.85 mm)

S = 3.6755, Model v_r = 1447 ft/s (441 m/s), Model M_r = 2.594, Model We = 616, Model Re = 1811

Figure 4.7 1-Propanol Droplet at x = 0.3626 in (9.21 mm)

S = 5.986, Model v_r = 1424 ft/s (434 m/s), Model M_r = 2.737, Model We = 597, Model Re = 1783

Figure 4.8 1-Propanol Droplet at x = 0.4163 in (10.57 mm)

S = 8.868, Model v_r = 1395 ft/s (425 m/s), Model M_r = 2.836, Model We = 572, Model Re = 1746
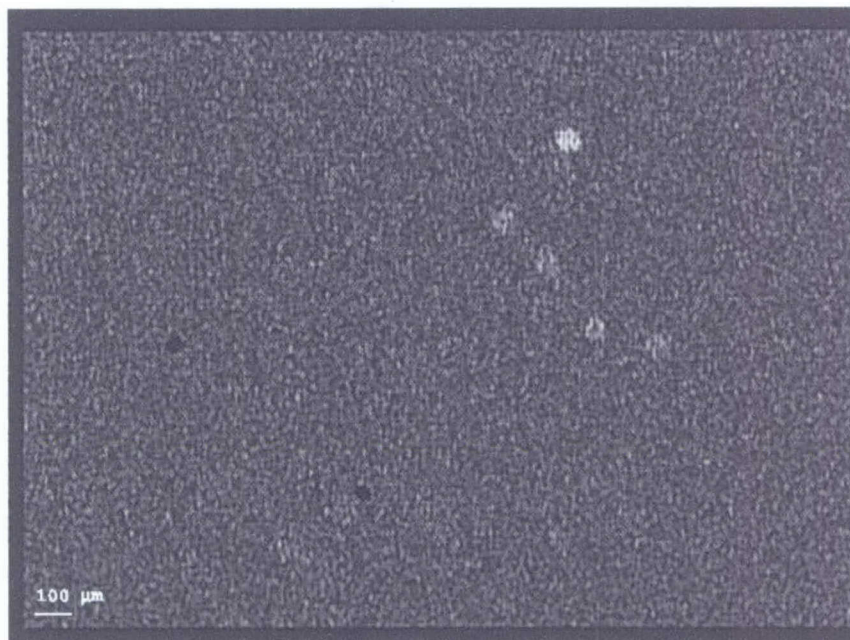
Figure 4.9 1-Propanol Droplet at x = 0.4754 in (12.08 mm)

S = 11.42, Model v_r = 1352 ft/s (412 m/s), Model M_r = 2.850,
Model We = 538, Model Re = 1692

Table 4.1 1-Propanol Droplet Data Summary

Figure	x in	S	Model v_r ft/s	Model M_r	Model We	Model Re
4.1	0.0109	0.0392	775.7	0.727	177	971
4.2	0.1109	0.2151	1373	1.641	555	1719
4.3	0.1430	0.3989	1425	1.861	598	1785
4.4	0.1818	0.7772	1450	2.082	619	1816
4.5	0.2622	2.2172	1459	2.434	626	1827
4.6	0.3089	3.6755	1447	2.594	616	1811
4.7	0.3626	5.986	1424	2.737	597	1783
4.8	0.4163	8.868	1395	2.836	572	1746
4.9	0.4754	11.42	1352	2.850	538	1692
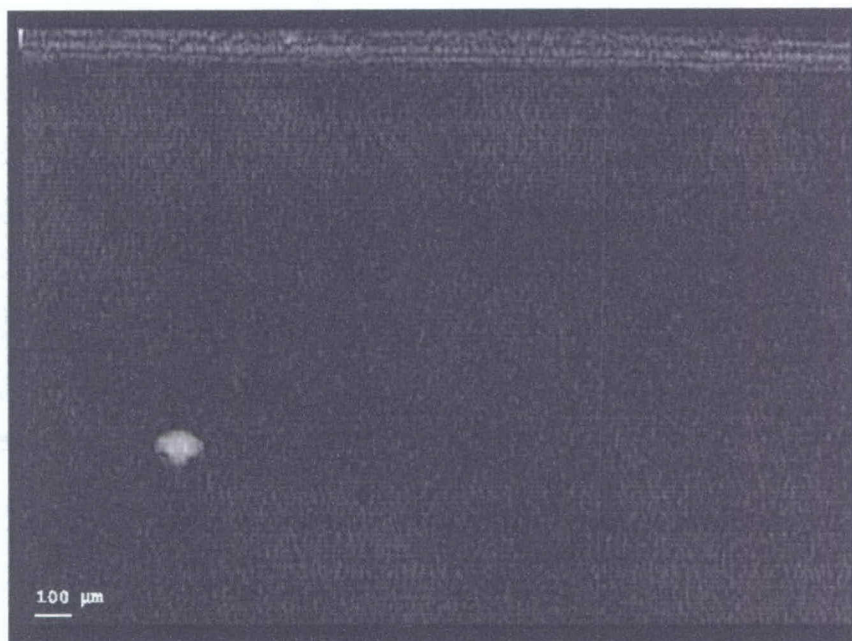
Figure 4.10 Ethanol Droplet at x = 0.0461 in (1.17 mm)

S = 0.1180, Model v_r = 956.2 ft/s (291 m/s), Model M_r = 0.936, Model We = 269, Model Re = 1197

Figure 4.11 Ethanol Droplet at x = 0.0692 in (1.76 mm)

S = 0.1965, Model v_r = 1207 ft/s (368 m/s), Model M_r = 1.272, Model We = 429, Model Re = 1512

Figure 4.12 Ethanol Droplet at x = 0.1129 in (2.87 mm)

S = 0.4955, Model v_r = 1375 ft/s (419 m/s), Model M_r = 1.654,
Model We = 557, Model Re = 1722

Figure 4.13 Ethanol Droplet at x = 0.1971 in (5.01 mm)

S = 2.1649, Model v_r = 1458 ft/s (444 m/s), Model M_r = 2.164,
Model We = 626, Model Re = 1826

Figure 4.14 Ethanol Droplet at x = 0.2622 in (6.66 mm)

S = 4.9000, Model v_r = 1459 ft/s (445 m/s), Model M_r = 2.434,
Model We = 626, Model Re = 1827
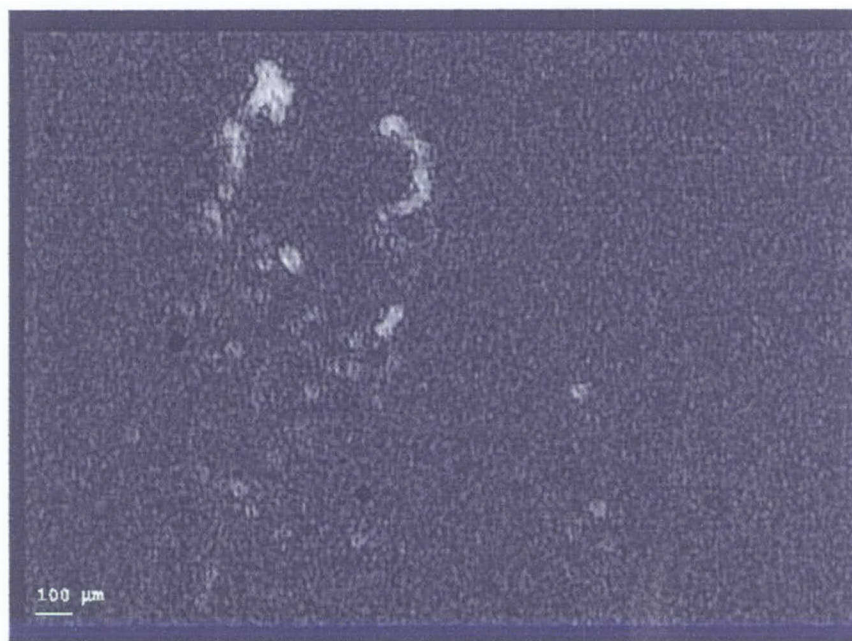
Figure 4.15 Ethanol Droplet at x = 0.2788 in (7.08 mm)

S = 5.8642, Model v_r = 1456 ft/s (444 m/s), Model M_r = 2.491,
Model We = 623, Model Re = 1823

Table 4.2 Ethanol Droplet Data Summary

Figure	x in	S	Model v_r ft/s	Model M_r	Model We	Model Re
4.10	0.0461	0.1180	956.2	0.936	269	1197
4.11	0.0692	0.1965	1207	1.272	429	1512
4.12	0.1129	0.4955	1375	1.654	557	1722
4.13	0.1971	2.1649	1458	2.164	626	1826
4.14	0.2622	4.9000	1459	2.434	626	1827
4.15	0.2788	5.8642	1456	2.491	623	1823
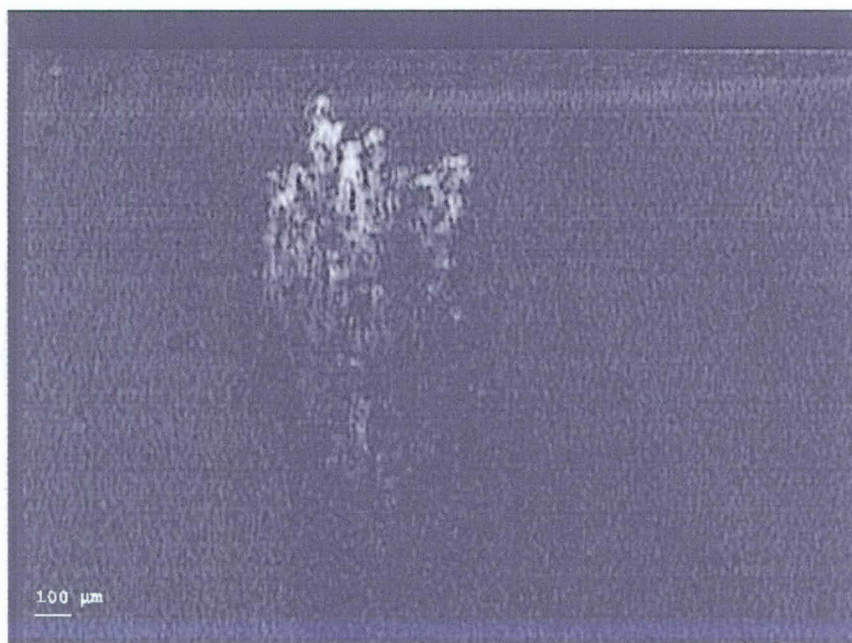
Figure 4.16 Methanol Droplet x = 0.0092 in (0.23 mm)

S = 0.1919, Model v_r = 765.5 ft/s (233 m/s), Model M_r = 0.716,
Model We = 173, Model Re = 959
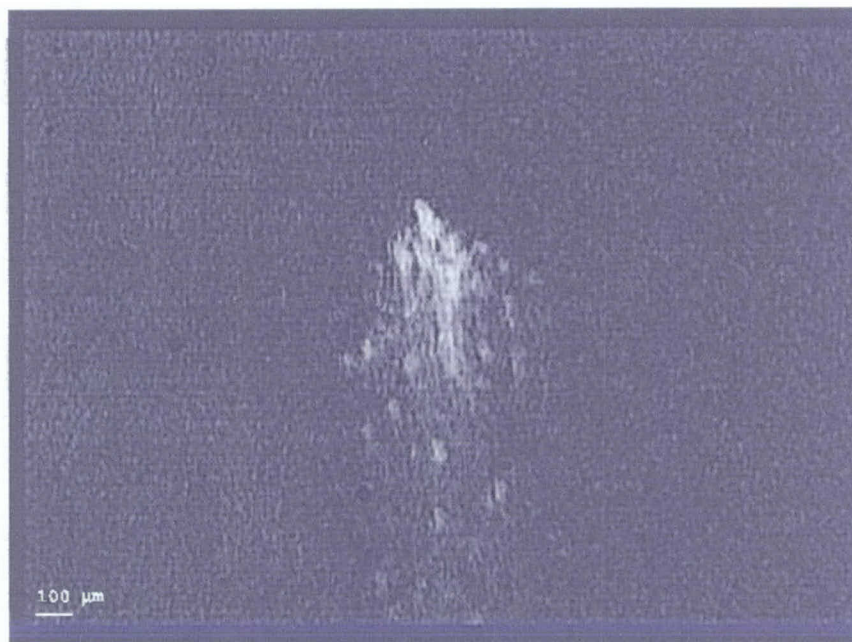
Figure 4.17 Methanol Droplet at x = 0.0843 in (2.14 mm)

S = 0.5674, Model v_r = 1286 ft/s (392 m/s), Model M_r = 1.415,
Model We = 487, Model Re = 1611
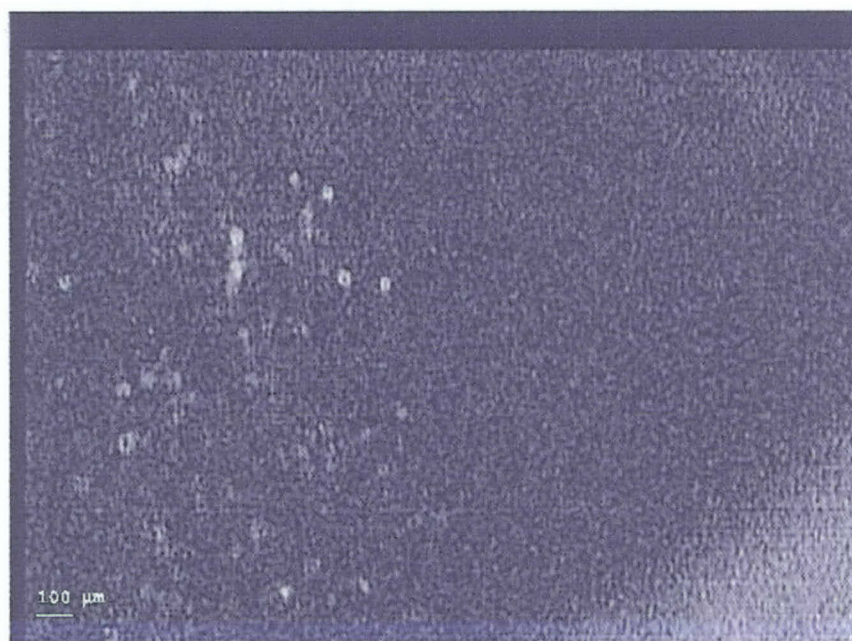
Figure 4.18 Methanol Droplet at x = 0.1407 in (3.57 mm)

S = 1.8878, Model v_r = 1424 ft/s (434 m/s), Model M_r = 1.846,
Model We = 597, Model Re = 1783

Table 4.3 Methanol Droplet Data Summary

Figure	x in	S	Model v_r ft/s	Model M_r	Model We	Model Re
4.16	0.0092	0.1919	765.5	0.716	173	959
4.17	0.0843	0.5974	1286	1.415	487	1611
4.18	0.1407	1.8878	1424	1.846	597	1783

DISCUSSION

Previous studies of the limit of superheat in liquids often used a heated bubble column with a slowly rising droplet.[12-15] Those droplets remained essentially spherical with an essentially uniform pressure distribution along the interface, and spontaneous nucleation occurred at a random point within the volume of the droplet. Once vapor had nucleated, vaporization spread rapidly throughout the liquid. The time for vaporization to progress through a droplet at the superheat limit would be on the order of one-tenth of the residence time of the droplet in the test section (as pointed out previously, the droplets in this work do not actually reach the superheat limit). In addition, the high acceleration of the droplets in the current experiment caused a non-uniform pressure distribution around the surface, and large aerodynamic forces were present which contributed to droplet breakup. To varying degrees in droplets of the three test fluids employed here, the droplet images suggest that spontaneous nucleation occurred at a fixed point and vaporization spread only partially through the liquid, with the remainder of the liquid fragmenting due to aerodynamic disruption.

The interface between the airflow and the droplet, like the interface between the two liquids in a bubble column, would remain microscopically smooth before droplet disruption,[14] inhibiting nucleation sites for heterogeneous boiling. Aerodynamic disruption of the surface of the droplet could, however, create such nucleation sites. A point of minimum pressure on the surface of the droplets existed on the leeward surface, possibly due to shock waves, which have been observed on rigid spheres at Mach numbers down to 0.9,[41] attached at the separation point of the turbulent wake, as well as due to the low pressure of the wake itself. Fluid in the bulk of the droplet near points of minimum pressure on the surface of the droplet would effectively experience higher degrees of superheat than the rest of the droplet, so that the spontaneous nucleation of vapor within the bulk liquid will occur earliest in portions of the droplet near points of low pressure. These portions of the droplet could flash vaporize while the rest of the droplet remains at a lower level of superheat, explosively fragmenting the remaining liquid. This explosive fragmentation due to superheat induced flash vaporization overwhelms the aerodynamic forces, masking whatever aerodynamic breakup mode would

otherwise exist. This is most apparent in the early fragmentation of the methanol droplets; the ethanol droplets also appear to have flash vaporized in the aft region, fragmenting, to a lesser extent than methanol, the unvaporized liquid.

Deformation of the droplet by the non-uniform pressure distribution, before the limit of superheat is reached by any of the liquid, will tend to drive the droplet towards a shape for which the pressure distribution would be more uniform. The slower the onset of superheating, the more uniform the pressure distribution on the surface of the droplet and, therefore, the more uniform the distribution of superheating will be throughout the liquid, and the longer the droplet liquid will persist before complete vaporization. This effect is the most pronounced in the droplets of 1-propanol, which appear to have vaporized uniformly with very little fragmentation, after extensive deformation while unsuperheated.

As can be seen from Table 5.1, for droplets with the more rapid increase in superheat level (see Fig. 2.14), the last observable fragments of droplets were recorded nearer the throat of the tunnel. Additionally, these rapidly superheated droplet fragments attained lower degrees of

superheat, lower relative Mach numbers, and lower Weber

numbers than less rapidly superheated droplet liquids.

Table 5.1 Comparison of Test Fluids

Test Fluid	x_{max} in	S_{max}	$M_{r,max}$	We_{max}
1-Propanol	0.4754	11.42	2.850	626
Ethanol	0.2788	5.86	2.491	626
Methanol	0.1407	1.89	1.846	597

CONCLUSION

By injecting droplets of three liquids with a range of vapor pressures into a freely expanding jet in a draw-down supersonic wind tunnel, the effects of liquid superheat on disruption and vaporization of smoothly accelerated droplets were examined. The choice of liquids, with similar densities and surface tensions, and variable but all low viscosities, allowed isolation of the effects of superheating from variation of effects from aerodynamic droplet breakup forces. A one dimensional computational model, based upon non-evaporating rigid spherical droplets was used to roughly estimate the expected flow conditions experienced by the droplets, and suggested that the droplets achieved supersonic relative velocities.

Images of droplets undergoing disruption suggest that nonuniform pressure distribution due to high relative flow velocities can initiate spontaneous nucleation of vaporization on the leeward side of droplets while some of the liquid is still below the superheat limit; the more uniform the pressure distribution on the surface of the droplet is, the higher the degree of superheat the droplet reaches before spontaneous nucleation of vaporization, the longer the majority of the droplet remains liquid, and the

larger the portion of the liquid which is vaporized rather than fragmented. Any degree of superheat appears to increase the violence of the breakup mode beyond that predicted by correlations to the Weber, Ohnesorge, and Reynolds numbers; the more rapidly the liquid in the droplet is superheated, the more the breakup is more violent than that predicted by the correlations.

FUTURE WORK

In order to more completely evaluate the effects of superheat on droplet breakup, work beyond the scope of the current research will be necessary. The most important step will be to determine actual droplet velocities for comparison with the model output. This could be accomplished with multiple exposure images of single droplets of each fluid in a laser sheet at known intervals of time. The observed position changes of the droplets over a known interval of time can be used to calculate average velocity over that distance. Once a sufficient population of data is obtained, a least squares fit velocity curve over the length of the test section can be calculated. From this, acceleration and estimates of drag can be determined. The large population of droplet position data can also be used to determine, from the rate at which droplets are observed at a given position downstream of the test section throat, an estimate of the effect of liquid superheating on the time until a droplet is fully disrupted.

A possible step to more fully characterize the effect of liquid superheat on disruption of a droplet at supersonic velocities relative to an air stream would be to

repeat the experiment of this study using additional test fluids with properties similar to the properties which are comparable among the fluids examined in this study and vapor pressure between that of ethanol and methanol, if such test fluids can be identified.

Once the effect of liquid superheat on droplet disruption and vaporization is more completely characterized, the behavior of the vapor should be studied. This could be accomplished through planar laser induced fluorescence of the vapor at an appropriate wavelength. The simplest method of accomplishing this is to add small quantities of a liquid which fluoresces well and is miscible with the fluids from this study, such as acetone, and observe the variation in the behavior of acetone vapor with different rates and degrees of superheating of the doped test fluid.

REFERENCES

[1]Curran, Edward T., "Scramjet Engines: The First Forty Years," *Journal of Propulsion and Power*, Vol. 17, No. 6, November-December, pp. 1138-1148.

[2]Townend, L.H., "Domain of the Scramjet," *Journal of Propulsion and Power*, Vol. 17, No. 6, November-December 2001, pp. 1205-1213.

[3]Waltrup, Paul J., "Upper Bounds on the Flight Speed of Hydrocarbon-Fueled Scramjet-Powered Vehicles," *Journal of Propulsion and Power*, Vol. 17, No. 6, November-December 2001, pp. 1199-1204.

[4]Kay, I.W., Peschke, W.T., and Guile, R.N., "Hydrocarbon-Fueled Scramjet Combustor Investigation," *Journal of Propulsion and Power*, Vol. 8, No. 2, March-April 1992, pp. 507-512.

[5]Powell, O.A., Ewards, J.T., Norris, R.B., and Numbers, K.E., "Development of Hydrocarbon-Fuels Scramjet Engines: The Hypersonic Technology (HyTech) Program," *Journal of Propulsion and Power*, Vol. 17, No. 6, November-December 2001, pp. 1170-1176.

[6]Colket, Meredith B., and Spadaccini, Louis J., "Scramjet Fuels Autoignition Study," *Journal of Propulsion and Power*, Vol. 17, No. 2, March-April 2001, pp. 315-323.

[7]Lander, H., and Nixon, A.C., "Endothermic Fuels for Hypersonic Vehicles," *J Aircraft*, Vol. 8, No. 4, 1971, pp. 200-207.

[8]Sobel, D.R., and Spadaccini, L.J., "Hydrocarbon Fuel Cooling Technologies for Advanced Propulsion," *Journal of Engineering for Gas Turbines and Power*, Vol. 119, April 1997, pp. 344-351.

[9]Lewis, Mark J., "Significance of Fuel Selection for Hypersonic Vehicle Range," *Journal of Propulsion and Power*, Vol. 17, No. 6, November-December 2001, pp. 1214-1221.

[10]Yanson, L.M., Phariss, M.R., and Hermanson, J.C., "Effects of Liquid Superheat on Droplet Disruption in a Supersonic Stream," *43rd AIAA Aerospace Sciences Meeting and Exhibit*, AIAA, Reno, NV, 2005, No. 2005-0351.

[11]Sornek, Rafal J., Dobashi, Ritsu, and Hirano, Toshisuke, "Effect of Turbulence on Vaporization, Mixing, and Combustion of Liquid-Fuel Sprays," *Combustion and Flame*, Vol. 120, 2000, pp. 479-491.

[12]Frost, D.L., "Dynamics of Explosive Boiling of a Droplet," *Physics of Fluids*, Vol. 31, No. 9, 1988, pp. 2554-2561.

[13]Nguyen, V.T., Furzeland, R.M., and Ijpelaar, M.J.M., "Rapid Evaporation at the Superheat Limit," *International Journal of Heat and Mass Transfer*, Vol. 31, No. 8, 1988, pp. 1687-1988.

[14]Ried, Robert C., "Superheated Liquids," *American Scientist*, Vol. 64, March-April 1976, pp. 146-156.

[15]Wakeshima, Hiromu, and Takata, Kazuo, "On the Limit of Superheat," *Journal of the Physical Society of Japan*, Vol. 13, No. 11, 1958, pp. 1398-1403.

[16]Lefebvre, Arthur, "Fifty Years of Gas Turbine Fuel Injection," *Atomization and Sprays*, Vol. 10, 2000, pp. 251-276.

[17]Hsiang, L.P., and Faeth, G.M., "Drop Deformation and Breakup due to Shock Wave Steady Disturbances," *International Journal of Multiphase Flow*, Vol. 21, No. 21, 1995, pp. 545-560.

[18]Joseph, D.D., Bellanger, J., and Beavers, G.S., "Breakup of a Liquid Drop Suddenly Exposed to a High-Speed Airstream," *International Journal of Multiphase Flow*, Vol. 25, 1999, pp. 1263-1303.

[19]Hwang, S.S., Liu, Z., and Reitz, R.D., "Breakup Mechanisms and Drag Coefficients of High-Speed Vaporizing Liquid Drops," *Atomization and Sprays*, Vol. 6, 1996, pp. 353-376.

[20]Shraiber, A.A., Podvysotky, A.M., and Dubrovsky, V.V., "Deformation and Breakup of Drops by Aerodynamic Forces," *Atomization and Sprays*, Vol. 6, 1996, pp. 667-692.

[21]Pilch, M., and Erdman, C.A., "Use of Breakup Time Data and Velocity History Data to Predict the Maximum Size of Stable Fragments for Acceleration-Induced Breakup of a Liquid Drop," *International Journal of Multiphase Flow*, Vol. 13, No. 6, 1987, pp. 741-757.

[22]Dai, Z., and Faeth, G.M., "Temporal Properties of Secondary Drop Breakup in the Multimode Breakup Regime," *International Journal of Multiphase Flow*, Vol. 27, 2001, pp. 217-236.

[23]Krzeczkowski, Stefan A., "Measurement of Liquid Droplet Disintegration Mechanisms," *International Journal of Multiphase Flow*, Vol. 6, 1980, pp. 227-239.

[24]Liu, Z., and Reitz, R.D., "An Analysis of the Distortion and Breakup Mechanisms of High Speed Liquid Drops," *International Journal of Multiphase Flow*, Vol. 23, No. 4, 1997, pp. 631-650.

[25]Simpkins, P.G., and Bales, E.L., "Water-drop Response to Sudden Accelerations," *Journal of Fluid Mechanics*, Vol. 55, No. 4, 1972, pp. 629-639.

[26]Wierzba, A., and Takayama, K., "Experimental Investigation of the Aerodynamic Breakup of Liquid Drops," *AIAA Journal*, Vol. 26, No. 11, 1988, pp. 1329-1335.

[27]Tan, M.J., and Bankoff, S.G., "On the Fragmentation of Drops," *Journal of Fluids Engineering*, Vol. 108, March 1986, pp. 109-114.

[28]Hirahara, H., and Kawahashi, M., "Experimental Investigation of Viscous Effects Upon a Breakup of Droplets in High-Speed Air Flow," *Experiments in Fluids*, No. 13, 1992, pp. 423-428.

[29]Krauss, William E., and Leadon, Bernard M., "Deformation Fragmentation of Water Drops due to Shock Wave Impact," *12th Structures, Structural Dynamics and Materials Conference*, AIAA/ASME, Anaheim, CA, No. 71-392.

[30]Ranger, A.A., and Nicholls, J.A., "Aerodynamic Shattering of Liquid Drops," *AIAA Journal*, February 1969, pp. 285-290.

[31]Hanson, A.R., Domich, E.G., and Adams, H.S., "Shock Tube Investigation of the Breakup of Drops by Air Blasts," *The Physics of Fluids*, Vol. 6, No. 8, August 1963, pp. 1070-1080.

[32]Williams, Forman A., "Atomization Processes and Ignition Criteria for Supersonic Combustion with Liquid Fuel Injection," *Astronautica Acta*, Vol. 15, 1970, pp. 547-557.

[33]Helenbrook, B.T., and Edwards, C.F., "Quasi-steady Deformation and Drag of Uncontaminated Liquid Drops," *International Journal of Multiphase Flow*, Vol. 28, 2002, pp. 1631-1657.

[34]Li, G.J., Dinh, T.N., and Theofanous, T.G., "An Experimental Study of Droplet Breakup in Supersonic Flow: The Effect of Long-Range Interactions," *42nd AIAA Aerospace Sciences Meeting and Exhibit*, AIAA, Reno, NV, 2004, No. 2004-968.

[35]Borisov, A.A., Gel'fand, B.E., Natanzon, M.S., and Kossov, O.M., "Droplet Breakup Regimes and Criteria for their Existence," *Journal of Engineering Physics*, Vol. 40, No. 1, 1981, pp. 44-49.

[36]Gelfand, B.E., "Droplet Breakup Phenomena in Flows with Velocity Lag," *Progress in Energy and Combustion Science*, Vol. 22, 1996, pp. 201-265.

[37]Tseng, Fan-Gang, "Micro-Droplet Generators," Ph.D. Dissertation, National Tsing Hua University, Taiwan, 2000.

[38]Fanning, David W., "Image Sharpening with a Laplacian Kernel," Fanning Consulting, Colorado, December 2003. [http://www.dfanning.com/ip_tips/sharpen.html. Accessed 3/7/05.]

[39]Lee, Cindy M., "Nonaqueous Phase Liquids in the Subsurface," Clemson University, South Carolina, January 2001. [http://www.bleonard.com/enviro/chemicals.xls. Accessed 3/7/05.]

[40]Reid, R. C., "Superheated Liquids", *American Scientist*, Vol. 64, March-April 1976.

[41]Charters, A.C., and Thomas, R.N., "The Aerodynamic Performance of Small Spheres from Subsonic to High Supersonic Velocities," *Journal of the Aeronautical Sciences*, October 1945, pp. 468-476.

[42]Fox, R.W., and McDonald, A.T., "External Incompressible Viscous Flow," *Introduction to Fluid Mechanics*, 5th ed., John Wiley & Sons, Inc., New York, 1998, pp. 444-450.

APPENDIX: MATLAB CODES

imageprocess.m

```
clear all;

[fname3, pname3] = uigetfile('*.tif', 'Open tiff of
     screw');

file3 = [pname3 fname3];

screw = imread(file3, 'tiff');

screw = double(screw);

screw = deinterlace(screw);

colormap(gray(255));

image(screw);

% Display GUI that determines the scaling of the images.

prompt = {'Threads per inch of the screw','Peak to peak
     spacing (pixels)'};

title = 'Scaling Information';

lines = 1;

def = {'80','85'};

hold = inputdlg(prompt,title,lines,def);

hold = char(hold);

hold = str2num(hold);

threads = 25400/hold(1);

pixels = hold(2);

scale = pixels*100/threads;
```

```
close;

cd (pname3);

[fname1, pname1] = uigetfile('*.tif', 'Open tiff file for
    file source path determination');

[fname2, pname2] = uigetfile('*.txt', 'Open txt file for
    file destination path determination');

t1 = fix(clock);

file1 = [pname1 fname1];

legend = imread(file1,'tiff');

legend = double(legend);

legend(455:456,20:20+round(scale)) = 255;

cd (pname1); directorynames = dir;

directorynames = char({directorynames.name});

directorynames = sortrows(directorynames);

cd Lens;

filenames = dir('*.tif');

filenames = char({filenames.name});

filenames = sortrows(filenames);

lensspots = zeros(480,640)+255;

for pic = 1:size(filenames,1);

    temp = imread(filenames(pic,:),'tiff');

    temp = double(temp);

    temp = deinterlace(temp);

    temp = 255-temp;
```

```
        mtemp = mean(mean(temp));

        h = find(temp > mtemp);

        Z = zeros(size(temp));

        Z(h) = 255;

        Z = (Z+lensspots)/2;

        h = find(Z < 255);

        lensspots(h) = 0;

for pixel = 1:4

        lensspots(:,1:pixel) = 0;

        lensspots(:,641-pixel:640) = 0;

        h = find(lensspots > 0);

        lensspots(h+1) = 255;

        lensspots(h-1) = 255;

        lensspots(h+480) = 255;

        lensspots(h-480) = 255;

end;

cd ..;

for position = 5:(size(directorynames)-2)

        cd (pname2);

        mkdir (directorynames(position,:));

        cd (pname1);

        cd (directorynames(position,:));

        subdirectorynames = dir;
```

```
subdirectorynames = char({subdirectorynames.name});

subdirectorynames = sortrows(subdirectorynames);

cd Window;

filenames = dir('*.tif');

filenames = char({filenames.name});

filenames = sortrows(filenames);

intensities = size(filenames,1);

for picture = 1:size(filenames,1);

    temp = imread(filenames(picture,:),'tiff');

    temp = double(temp);

    temp = deinterlace(temp);

    temp = lensfunction(temp,lensspots);

    intensities(picture) = mean(mean(temp));

end;

cd ..;

for run = 3:(size(subdirectorynames)-1)

    cd (pname2);

    cd (directorynames(position,:));

    mkdir (subdirectorynames(run,:));

    cd (pname1);

    cd (directorynames(position,:));

    cd (subdirectorynames(run,:));

    picfilenames = dir('*.tif');
```

```
picfilenames = char({picfilenames.name});

picfilenames = sortrows(picfilenames);

for picture = 1:size(picfilenames)

    pic =
        imread(picfilenames(picture,:),'tiff');

    pic = double(pic);

    pic = deinterlace(pic);

    pic = lensfunction(pic,lensspots);

    picintensity = mean(mean(pic));

    h =  matchintensity(intensities,
        picintensity);

    cd ..;

    cd Window;

    winpic = imread(filenames(h,:),  'tiff');

    winpic = double(winpic);

    winpic = deinterlace(winpic);

    winpic = lensfunction(winpic,lensspots);

    cd ..;

    cd (pname2);

    cd (directorynames(position,:));

    cd (subdirectorynames(run,:));

    winpic =
        winpic*(picintensity/intensities(h));

    pic = motionfunction(pic,winpic,16,6);
```

```
                  pic = sharpen(pic);

                  pic = pic + legend;

                  pic = uint8(pic);

                  imwrite(pic, picfilenames(picture,:),
                      'tiff');

                  picfilenames(picture,:)

                  cd (pname1);

                  cd (directorynames(position,:));

                  cd (subdirectorynames(run,:));

            end;

            cd ..;

      end;

      cd ..;

end;

t2 = fix(clock);

days = t2(3)-t1(3);

hours = t2(4)-t1(4);

minutes = t2(5)-t1(5);

seconds = t2(6)-t1(6);

if seconds < 0

      seconds = 60+seconds;

      minutes = minutes-1;

end;
```

```
if minutes < 0

    minutes = 60+minutes;

    hours = hours-1;

end;

if hours < 0

    hours = 24+hours;

    days = days-1;

end;

msgbox(sprintf('Image processing complete.\n\nTotal elapsed
    runtime was %g:%g:%g.',hours,minutes,seconds));
```

deinterlace.m

```
function out = deinterlace(in);

odd = in;

even = in;

rows = size(in,1);

for count = 2:rows-1;

    if max(2 == factor(count)) == 1

        odd(count,:) = (odd(count-1,:) +
            odd(count+1,:))/2;

    else

        even(count,:) = (even(count-1,:) +
            even(count+1,:))/2;

    end

end
```

```
even(1,:) = even(2,:);

if max(2 == factor(rows)) == 1

    odd(rows,:) = odd(rows-1,:);

else

    even(rows,:) = even(rows-1,:);

end

if mean(mean(even)) > mean(mean(odd))

    out = even;

else

    out = odd;

end
```

lensfunction.m

```
function OUT = lensfunction(IN,spots)

in = mean(mean(IN(241:460,21:620)));

IN = IN-spots;

h = find(IN<0);

IN(h) = in;

OUT = IN;
```

matchintensity.m

```
function out =
    matchintensity(intensitiesvector,intensityscalar)

a = ones(size(intensitiesvector))*intensityscalar;

out = find(min(abs(a-intensitiesvector))==
    (abs(a-intensitiesvector)));
```

motionfunction.m

```
function out = motionfunction(in,B,rowcrop,columncrop)

C = B(rowcrop+1:480-rowcrop,columncrop+1:640-columncrop);

for r = 1:2*rowcrop;

    for c = 1:2*columncrop;

            S(r,c) = sum(sum(abs(in(r:479-
                (2*rowcrop)+r,c:639-(2*columncrop)+c)-C)));

    end;

end;

h = min(min(S));

[i,j] = find(S==h);

B = zeros(size(in));

B(i:i+479-(2*rowcrop),j:j+639-(2*columncrop)) = C;

A = zeros(size(in));

A(i:i+479-(2*rowcrop),j:j+639-(2*columncrop)) =
    in(i:i+479-(2*rowcrop),j:j+639-(2*columncrop));

out = abs(A-B);

mout = max(max(out));

out = 255/mout*out;
```

sharpen.m

```
function out = sharpen(in);

smoothed = medianA(in);

filtered = laplacian(smoothed);
```

```
filtered = filtered - min(min(filtered));

filtered = filtered * 255/max(max(filtered));

sharpened = smoothed + filtered;

sharpened = sharpened - min(min(sharpened));

sharpened = sharpened * 255/max(max(sharpened));

out = sharpened;
```

medianA.m

```
function out = medianA(in);

[height,width] = size(in);

in = double(in);

out = zeros(size(in));

%Center area

out(3:height-2,3:width-2) = 1/13*(in(1:height-4,3:width-2)
     + in(2:height-3,2:width-3) + in(2:height-3,3:width-2)
     + in(2:height-3,4:width-1) + in(3:height-2,1:width-4)
     + in(3:height-2,2:width-3) + in(3:height-2,3:width-2)
     + in(3:height-2,4:width-1) + in(3:height-2,5:width) +
     in(4:height-1,2:width-3) + in(4:height-1,3:width-2) +
     in(4:height-1,4:width-1) + in(5:height,3:width-2));

%One pixel away from a horizontal edge, center row

out(2,3:width-2) = 1/12*(in(1,2:width-3) + in(1,3:width-2)
     + in(1,4:width-1) + in(2,1:width-4) + in(2,2:width-3)
     + in(2,3:width-2) + in(2,4:width-1) + in(2,5:width) +
     in(3,2:width-3) + in(3,3:width-2) + in(3,4:width-1)
     in(4,3:width-2));

out(height-1,3:width-2) = 1/12*(in(height-3,3:width-2) +
     in(height-2,2:width-3) + in(height-2,3:width-2) +
     in(height-2,4:width-1) + in(height-1,1:width-4) +
     in(height-1,2:width-3) + in(height-1,3:width-2) +
     in(height-1,4:width-1) + in(height-1,5:width) +
```

```
        in(height,2:width-3) + in(height,3:width-2) +
        in(height,4:width-1));

%One pixel away from a vertical edge, center column

out(3:height-2,2) = 1/12*(in(1:height-4,2) +
        in(2:height-3,1) + in(2:height-3,2) + in(2:height-3,3)
        + in(3:height-2,1) + in(3:height-2,2) +
        in(3:height-2,3) + in(3:height-2,4) + in(4:height-1,1)
        + in(4:height-1,2) + in(4:height-1,3) +
        in(5:height,2));

out(3:height-2,width-1) = 1/12*(in(1:height-4,width-1) +
        in(2:height-3,width-2) + in(2:height-3,width-1) +
        in(2:height-3,width) + in(3:height-2,width-3) +
        in(3:height-2,width-2) + in(3:height-2,width-1) +
        in(3:height-2,width) + in(4:height-1,width-2) +
        in(4:height-1,width-1) + in(4:height-1,width) +
        in(5:height,width-1));

%One pixel away from corner in both directions

out(2,2) = 1/11*(in(1,1) + in(1,2) + in(1,3) + in(2,1) +
        in(2,2) + in(2,3) + in(2,4) + in(3,1) + in(3,2) +
        in(3,3) + in(4,2));

out(2,width-1) = 1/11*(in(1,width-2) + in(1,width-1) +
        in(1,width) + in(2,width-3) + in(2,width-2) +
        in(2,width-1) + in(2,width) + in(3,width-2) +
        in(3,width-1) + in(3,width) + in(4,width-1));

out(height-1,2) = 1/11*(in(height-3,2) + in(height-2,1) +
        in(height-2,2) + in(height-2,3) + in(height-1,1) +
        in(height-1,2) + in(height-1,3) + in(height-1,4) +
        in(height,1) + in(height,2) + in(height,3));

out(height-1,width-1) = 1/11*(in(height-3,width-1) +
        in(height-2,width-2) + in(height-2,width-1) +
        in(height-2,width) + in(height-1,width-3) +
        in(height-1,width-2) + in(height-1,width-1) +
        in(height-1,width) + in(height,width-2) +
        in(height,width-1) + in(height,width));

%Horizontal edge, center row
```

```
out(1,3:width-2) = 1/9*(in(1,1:width-4) + in(1,2:width-3) +
    in(1,3:width-2) + in(1,4:width-1) + in(1,5:width) +
    in(2,2:width-3) + in(2,3:width-2) + in(2,4:width-1) +
    in(3,3:width-2));
out(height,3:width-2) = 1/9*(in(height-2,3:width-2) +
    in(height-1,2:width-3) + in(height-1,3:width-2) +
    in(height-1,4:width-1) + in(height,1:width-4) +
    in(height,2:width-3) + in(height,3:width-2) +
    in(height,4:width-1) + in(height,5:width));

%Vertical edge, center column

out(3:height-2,1) = 1/9*(in(1:height-4,1) +
    in(2:height-3,1) + in(2:height-3,2) + in(3:height-2,1)
    + in(3:height-2,2) + in(3:height-2,3) +
    in(4:height-1,1) + in(4:height-1,2) + in(5:height,1));

out(3:height-2,width) = 1/9*(in(1:height-4,width) +
    in(2:height-3,width-1) + in(2:height-3,width) +
    in(3:height-2,width-2) + in(3:height-2,width-1) +
    in(3:height-2,width) + in(4:height-1,width-1) +
    in(4:height-1,width) + in(5:height,width));

%One pixel in horizontally from corners

out(1,2) = 1/8*(in(1,1) + in(1,2) + in(1,3) + in(1,4) +
    in(2,1) + in(2,2) + in(2,3) + in(3,2));

out(1,width-1) = 1/8*(in(1,width-3) + in(1,width-2) +
    in(1,width-1) + in(1,width) + in(2,width-2) +
    in(2,width-1) + in(2,width) + in(3,width-1));

out(height,2) = 1/8*(in(height-2,2) + in(height-1,1) +
    in(height-1,2) + in(height-1,3) + in(height,1) +
    in(height,2) + in(height,3) + in(height,4));

out(height,width-1) = 1/8*(in(height-2,width-1) +
    in(height-1,width-2) + in(height-1,width-1) +
    in(height-1,width) + in(height,width-3) +
    in(height,width-2) + in(height,width-1) +
    in(height,width));

%One pixel in vertically from corners
```

```
out(2,1) = 1/8*(in(1,1) + in(1,2) + in(2,1) + in(2,2) +
     in(2,3) + in(3,1) + in(3,2) + in(4,1));
out(2,width) = 1/8*(in(1,width-1) + in(1,width) +
     in(2,width-2) + in(2,width-1) + in(2,width) +
     in(3,width-1) + in(3,width) + in(4,width));

out(height-1,1) = 1/8*(in(height-3,1) + in(height-2,1) +
     in(height-2,2) + in(height-1,1) + in(height-1,2) +
     in(height-1,3) + in(height,1) + in(height,2));

out(height-1,width) = 1/8*(in(height-3,width) +
     in(height-2,width-1) + in(height-2,width) +
     in(height-1,width-2) + in(height-1,width-1) +
     in(height-1,width) + in(height,width-1) +
     in(height,width));

%Corners

out(1,1) = 1/6*(in(1,1) + in(1,2) + in(1,3) + in(2,1) +
     in(2,2) + in(3,1));

out(1,width) = 1/6*(in(1,width-2) + in(1,width-1) +
     in(1,width) + in(2,width-1) + in(2,width) +
     in(3,width));

out(height,1) = 1/6*(in(height-2,1) + in(height-1,1) +
     in(height-1,2) + in(height,1) + in(height,2) +
     in(height,3));

out(height,width) = 1/6*(in(height-2,width) +
     in(height-1,width-1) + in(height-1,width) +
     in(height,width-2) + in(height,width-1) +
     in(height,width));
```

laplacian.m

```
function out = laplacian(in);

[height,width] = size(in);

in = double(in);

out = zeros(size(in));
```

```
out(2:height-1,2:width-1) = -(in(1:height-2,1:width-2) +
    in(1:height-2,2:width-1) + in(1:height-2,3:width) +
    in(2:height-1,1:width-2) - 8*in(2:height-1,2:width-1)
    + in(2:height-1,3:width) + in(3:height,1:width-2) +
    in(3:height,2:width-1) + in(3:height,3:width));

out(1,2:width-1) = -(in(1,1:width-2) - 5*in(1,2:width-1) +
    in(1,3:width) + in(2,1:width-2) + in(2,2:width-1) +
    in(2,3:width));

out(height,2:width-1) = -(in(height,1:width-2) -
    5*in(height,2:width-1) + in(height,3:width) +
    in(height-1,1:width-2) + in(height-1,2:width-1) +
    in(height-1,3:width));

out(2:height-1,1) = -(in(1:height-2,1) - 5*in(2:height-1,1)
    + in(3:height,1) + in(1:height-2,2) + in(2:height-1,2)
    + in(3:height,2));

out(2:height-1,width) = -(in(1:height-2,width) -
    5*in(2:height-1,width) +  in(3:height,width) +
    in(1:height-2,width-1) + in(2:height-1,width-1) +
    in(3:height,width-1));

out(1,1) = 3*in(1,1) -(in(1,2) + in(2,1) + in(2,2));

out(1,width) = 3*in(1,width) -(in(1,width-1) + in(2,width)
    + in(2,width-1));

out(height,1) = 3*in(height,1) -(in(height-1,1) +
    in(height,2) + in(height-1,2));

out(height,width) = 3*in(height,width) -(in(height-1,width)
    + in(height,width-1) + in(height-1,width-1));
```